Nat Commun. Author manuscript; available in PMC 2014 November 08.

Published in final edited form as:
Nat Commun. ; 5: 3795. doi:10.1038/ncomms4795.

S100A11 is required for efficient plasma membrane repair and survival of invasive cancer cells

Jyoti K. Jaiswal[1,*], **Stine P. Lauritzen**[5], **Luana Scheffer**[1], **Masakiyo Sakaguchi**[2], **Jakob Bunkenborg**[3], **Sanford M. Simon**[4], **Tuula Kallunki**[5], **Marja Jäättelä**[5], and **Jesper Nylandsted**[5,*]

[1]Children's National Medical Center, Center for Genetic Medicine Research, 111 Michigan Avenue, NW, Washington, DC 20010-2970

[2]Okayama University, Graduate School of Medicine, Dentistry and Pharmaceutical Sciences Kitaku, Shikajta-cho 2-5-1, Okayama 700-8558, Japan

[3]Department of Clinical Biochemistry, Copenhagen University Hospital Hvidovre, DK-2650 Hvidovre Denmark

[4]Laboratory of Cellular Biophysics, The Rockefeller University,1230 York Avenue, New York, NY 10065

[5]Unit for Cell Death and Metabolism, Danish Cancer Society Research Center, DK-2100 Copenhagen, Denmark

Abstract

Cell migration and invasion require increased plasma membrane dynamics and ability to navigate through dense stroma, thereby exposing plasma membrane to tremendous physical stress. Yet, it is largely unknown how metastatic cancer cells acquire an ability to cope with such stress. Here we show that S100A11, a calcium-binding protein up-regulated in a variety of metastatic cancers, is essential for efficient plasma membrane repair and survival of highly motile cancer cells. Plasma membrane injury-induced entry of calcium into the cell triggers recruitment of S100A11 and Annexin A2 to the site of injury. We show that S100A11 in a complex with Annexin A2 helps reseal the plasma membrane by facilitating polymerization of cortical F-actin and excision of the damaged part of the plasma membrane. These data reveal plasma membrane repair in general and S100A11 and Annexin A2 in particular, as new targets for the therapy of metastatic cancers.

[*]Correspondence: JKJ – jkjaiswal@cnmc.org; JN - jnl@cancer.dk.

Author Contributions: J.K.J. and J.N. conceived the study, designed and executed the experiments analyzed data and wrote the manuscript. S.P.L., L.S., J.B. and T.K. helped to carry out the experiments. M.S. contributed novel reagents. S.M.S. and M.J. contributed to the experimental design and manuscript writing.

The authors declare no financial or other conflicts of interest.

Europe PMC Funders Author Manuscripts

INTRODUCTION

Even in the protective environment of a tissue, various mechanical and chemical stresses can damage a cell's plasma membrane. Accordingly, defect in plasma membrane repair (PMR) is associated with diseases such as muscular dystrophy[1], diabetes[2], and Chediak Higashi Syndrome[3]. Damaged membrane can be repaired by spontaneous lipid flow across the injured site, outward budding of the damaged membrane, and by exocytic fusion of lysosomes and other cytosolic vesicles[4-6].

PMR is triggered by Ca^{2+} influx at the injury site, which facilitates cytoskeletal reorganization and membrane fusion events. Cortical cytoskeleton associated with the plasma membrane creates membrane tension, which prevents spontaneous resealing of the membrane[7]. Thus, spatial and temporal remodeling of cortical cytoskeleton at the wound site is essential for efficient PMR[8]. In Xenopus oocytes and Drosophila embryos, membrane injury-induced Ca^{2+} influx triggers a decrease in membrane tension through depolymerization of cortical actin cytoskeleton and subsequent formation of a dynamic actin-myosin ring, which contracts and closes the wound in a purse string manner[9,10]. Additionally, PMR requires a coordinated interaction between annexin-containing multiprotein complexes and the inner phospholipid surface to seal the rupture[4]. The members of the annexin protein family function as intracellular Ca^{2+} sensors. They interact with multiple proteins and distinct anionic phospholipids to promote membrane segregation, vesicle trafficking, vesicle fusion as well as membrane and cytoskeletal organization in a Ca^{2+}-dependent manner[11, 12]. Annexins ANXA1, ANXA6 and ANXA5 regulate PMR by binding the wounded cell membrane and initiating membrane fusion events or forming a protein lattice[13-15], whereas ANXA2 has been associated with the repair of plasma membrane as well as intracellular vesicle fusion[16, 17]. Ca^{2+} increase also causes members of the S100 family of EF-hand Ca^{2+} binding motif-containing proteins to undergo a conformational change, which exposes a hydrophobic domain of S100 proteins that can interact with the NH_2-terminal region of some annexins, such as ANXA1 and ANXA2[18]. This interaction is suggested to facilitate close apposition of adjacent phospholipid membranes during a membrane fusion event[19]. However, a role of S100 proteins in cell membrane repair has not been investigated.

Increased membrane dynamics and invasion through dense extracellular matrix would expose metastatic cells to membrane stress. Furthermore, malignant transformation is associated with altered membrane stiffness, which together with altered membrane dynamics can lead to stretch-induced membrane pores/ruptures[20]. Yet, the role of PMR in cancer metastasis has not been investigated. It has been reported that annexin-binding protein S100A11 (also known as calgizzarin or metastatic lymph node gene 70 protein) is enriched in pseudopodia of metastatic cancer cells and is essential for the formation of actin-dependent pseudopodial protrusions and tumor cell migration[21]. S100A11 expression is increased in various tumors, and is associated with tumor metastasis as well as poor prognosis in pancreatic, lung and colon cancers[22-27].

We have recently shown that induction of invasive phenotype in MCF7 breast cancer cells by NH_2-terminally truncated 95 kDa form of ErbB2 (p95ErbB2), which mimics the

constitutively active cleaved form of ErbB2 oncoprotein commonly found in aggressive breast cancers, is associated with up-regulation of S100A11 at the lysosome[28, 29]. Expression of p95ErbB2 increases invasiveness and mechanical activity of MCF7[29-31]. We thus evaluated if p95ErbB2 increases plasma membrane injury and if interaction of S100A11 with annexins and lysosome facilitates enhanced PMR. We find that S100A11 depletion does not alter motility, but prevents invasiveness of the MCF7-p95ErbB2 cells by compromising the PMR ability of MCF7-p95ErbB2 cells. S100A11 was not required for injury triggered lysosome fusion with the plasma membrane. Instead, we found that *in vivo*, S100A11 forms a complex with annexin A2 at the site of injury which facilitates local remodeling of actin cytoskeleton and excision of injured cell membrane. We have thus uncovered an increased need of PMR for invasive cancer cells and show a novel mechanism by which S100A11 helps the invasive cancer cells maintain their plasma membrane integrity.

RESULTS

S100A11 protects from invasion associated cell membrane stress

We have previously identified S100A11 as a lysosome-associated protein, whose abundance in the lysosomal fraction was increased approximately 3-fold upon p95ErbB2 expression[28]. Notably, p95ErbB2 expression in MCF7 cells increased S100A11 expression by 3-fold at mRNA and protein levels, the majority of which was localized diffusely in the cytosol (Fig. 1b, Supplementary Figure 1a and b). This up-regulation of S100A11 is mediated by signaling due to p95ErbB2 overexpression, as treating these cells with the MAPK/ERK inhibitor (PD98059) reduced S100A11 protein level in a dose dependent manner (Fig. 1c).

Signaling by the truncated active form of ErbB2 oncoprotein (p95ErbB2) significantly enhances cell motility, membrane ruffling, formation of protrusions, and invasiveness of MCF7 breast cancer cells[29, 32]. This increased activity could lead to increased plasma membrane damage, which may be repaired with help from the S100 binding proteins-Annexins[4, 5, 14, 15]. We thus investigated if p95ErbB2-induced invasive phenotype of MCF7 cells was associated with increased damage to their plasma membrane. Ca^{2+}-dependent recruitment of ANXA1-GFP to the plasma membrane has been shown to be a marker for plasma membrane damage[33]. We found that compared to 8% of control cells, 40% of MCF7-p95ErbB2 cells displayed extensive plasma membrane association of ANXA1-GFP (Fig. 1a, and Supplementary Movie 1). As changes in phosphoinositide metabolism and increased spontaneous Ca^{2+}-transients can also increase association of ANXA1-GFP to the cell membrane we used an independent assay for spontaneous injury and repair of plasma membrane – this involved monitoring the influx of cell membrane impermeable dye (Hoechst-3342) into live cells. MCF7-p95ErbB2 cells were 5-fold more resistant to Hoechst-3342 influx than vector-transfected control cells (Fig. 1e). Taken together with the results of ANXA1-GFP reporter, reduced dye leakage indicates that MCF7-p95ErbB2 cells are protected from the effects of increased plasma membrane injury by increased PMR (Fig. 1a). We thus tested if S100A11 over expression protects MCF7-p95ErbB2 cells from increased membrane damage, by depleting these cells of S100A11. S100A11 depletion did not alter the growth ability of the cells as they showed similar cell cycle profile

(Supplementary Figure 1g). However, this increased the cell membrane damage which was indicated by the increase in number of cells with membrane recruited ANXA1 (Fig. 1a), and an increase in number of dead cells measured by their ability to exclude propidium iodide (PI) (Fig. 1d). Further, S100A11 depletion in MCF7-vector and MCF7-p95ErbB2 cells resulted in a greater dye influx in the MCF7-p95ErbB2 (4-fold) as compared to the MCF7-vector cells (1.7-fold) (Fig. 1f). While increased Hoechst 3342 labeling requires dye to enter the nucleus, we tested if any of the dye entry could be due to increased endocytic/pinocytic uptake. For this we tested endocytosis and pinocytosis using lipophilic membrane dye FM1-43 and fluorescence dextran respectively. We found no significant difference in endocytosis or pinocytosis following S100A11 depletion in HeLa or MCF7-p95ErbB2 cells (Supplementary Figure 1c and d) similarly there was no significant difference between the endocytic rate between MCF7-vector and MCF7-p95ErbB2 cells (Supplementary Figure 1e). Additionally, we found that within 2 min of inhibiting PMR (by the removal of Ca^{2+} from the medium) there was significantly more influx of Hoechst 3342 in MCF7-p95ErbB2 than MCF7-vector cells and this increased dye influx continued linearly thereafter (Fig. 1g) such that by 2 hours over 65% of MCF7-p95ErbB2 cells died, as compared to only 15% of MCF7-vector cells (Fig. 1h - plot). Taken together, these data suggest that p95ErbB2-induced transformation results in increased membrane stress and damage, which can be effectively compensated by S100A11- and Ca^{2+}-dependent PMR.

S100A11 enhances repair of large plasma membrane injuries

Next, we investigated if S100A11 assists in the repair of large plasma membrane injuries. In the first assay, cells were injured by rolling glass beads and then allowed to heal for 5 min. MCF7-p95ErbB2 cells were twice as efficient as MCF7-vector cells at healing from glass bead injury and this efficacy was dependent on the expression of S100A11 in MCF7-p95ErbB2 cells (Fig. 2a). In the second assay we examined the kinetics of PMR by monitoring the entry of membrane impermeable FM1-43 dye into cells following a laser-induced local injury to the cell membrane. MCF7-p95ErbB2 cells repaired significantly faster than the MCF7-vector cells and the repair efficacy of MCF7-p95ErbB2 cells was compromised by the lack of S100A11 expression (Fig. 2b). As an independent test for the role of S100A11 in PMR, we carried out laser-injury of HeLa cervical carcinoma cells expressing ANXA1-GFP alone or together with S100A11-RFP. In S100A11-RFP-expressing cells (cell #1 in Fig. 2c and Supplementary Movie 2), ANXA1-GFP localized to the site of injury within 10 sec of the laser wound and was cleared again within a minute. In S100A11-RFP-negative cells, ANXA1-GFP localized to the proximity of the injury within 10 sec but remained localized there even 90 seconds after the injury indicating a delay/failure of this cell to heal (cell #2 in Fig. 2c and Supplementary Movie 2). These data suggest that S100A11 is not involved in the initial recruitment of ANXA1 to the membrane wound, but instead, enhances the capacity of cells to complete the healing process. The protective ability of ectopic S100A11 in HeLa cells was consistent in a complementary assay where vector- and S100A11-transfected HeLa cells were allowed to repair for 10 min after cell membrane injury by scrape wounding (Fig. 2d). Similar to the MCF7 cells, depletion of the endogenous S100A11 in HeLa cells (using 3 independent siRNAs) significantly reduced cell viability (Fig. 2e).

Taken together, these data support the hypothesis that S100A11 is essential for the efficient repair of externally induced large plasma membrane damage. When imaging the damaged MCF7-p95ErbB2 cells or S100A11-transfected HeLa cells, we frequently observed that the injured part of the cell membrane was excised from the rest of the cell (Fig. 2b and 2c, cell #1; Supplementary Movie 2). Such excision was not observed in MCF7-vector cells or in S100A11-depleted MCF7-p95ErbB2 cells suggesting that S100A11 may be involved in the excision of the damaged membrane.

S100A11 is not required for injury-triggered lysosomal exocytosis

Calcium-triggered exocytic fusion of lysosomes with the plasma membrane has been implicated in PMR[5]. As S100A11 can associate with lysosomes[28], we next examined the putative role of S100A11 in PMR by lysosomal exocytosis. MCF7-p95ErbB2 cells in culture displayed over 2-fold more lysosome-associated membrane protein 1 (LAMP1) on the cell surface than MCF7-vector cells (Fig. 3a, white bars). S100A11 depletion caused a 2-fold increase in cell surface LAMP1 levels in MCF7-vector and MCF7-p95ErbB2 cells, suggesting that S100A11 also has an impact on basal lysosomal exocytosis in MCF7-vector and MCF7-p95ErbB2 cells (Figure 3a, black bars). S100A11 depletion also significantly increased basal level of cell surface LAMP1 in HeLa cells (Fig. 3b and Supplementary Figure 1f). Calcium ionophore treatment of HeLa cells caused a 5-fold increase in cell surface LAMP1 and depletion of S100A11 did not alter this fold change (Fig. 3c).

In another approach, we directly monitored the exocytic activity of FITC-dextran-labeled lysosomes (bursts of dextran release to the extracellular space) in untreated cells and in response to laser injury by total internal reflection (TIRF) microscopy[34, 35]. In agreement with increased cell surface LAMP1 staining (Fig. 3a), the basal exocytic activity was doubled by the expression of p95ErbB2 (Fig. 3d). Laser injury triggered an S100A11-independent 4-fold increase in the number of lysosome exocytosis events, and these fusions spread throughout the cell and not specifically around the injury site (Fig. 3d and 3e). Thus, S100A11 is not needed for lysosomal exocytosis and the increased basal lysosomal exocytosis in S100A11-depleted cells may reflect an increased influx of Ca^{2+} as a consequence of defective PMR.

Ca^{2+}-triggers S100A11-ANXA2 interaction at the site of repair

To gain insight into the mechanism by which S100A11 regulates PMR, we monitored localization of S100A11 and potential binding partners ANAX1 and ANXA2. Within 30 sec of the laser injury of MCF7-p95ErbB2 cells expressing GFP- and RFP-tagged pair of these proteins, ANXA1 and S100A11 began to accumulate around the site of injury, reaching a maximum accumulation by 150 sec (Fig. 4a, Supplementary Figure 2a and b, Supplementary Movie 3). As the repair proceeded, ANXA1 localized to the injured membrane that was eventually excised, whereas S100A11 was localized to the repairing cell membrane (Fig. 4a, Supplementary Figure 2a and b, Supplementary Movie 3). After repair and excision of the injured membrane, S100A11 diffused back into the cytosol within the next 100 sec, while ANXA1 remained at the injured and excised membrane (Supplementary Figure 2a, and Supplementary Movie 3). In the absence of Ca^{2+}, ANXA1 and S100A11 leaked out of the damaged cell failing to accumulate at the site of injury (Supplementary Figure 2c).

Upon injury, simultaneously with S100A11, ANXA2 also accumulated at the injury site (Fig. 4b, 4c). However, unlike ANXA1, following injury-triggered accumulation ANXA2 was cleared simultaneously with S100A11 at the repairing membrane in injured MCF7-p95ErbB2 (Fig. 4b - plot) and HeLa cells (Fig. 4c - plot and Supplementary Movie 4). Depletion of ANXA2 in HeLa cells by using ANXA2-siRNA (Supplementary Figure 2d) prevented the accumulation of S100A11 (Fig. 4d), and vice versa depletion of S100A11 (Fig. 2e) prevented the accumulation of ANXA2 at the repair site (Fig. 4e). These results together with the reported ability of ANXA2 and S100A11 to interact with each other in vitro[36] suggested that ANXA2 and S100A11 are recruited to the site of repair as a complex. Thus, it is interesting to note that akin to S100A11, the expression of ANXA2 was significantly up-regulated by p95ErbB2 in MCF7 cells (Supplementary Figure 2d).

To investigate the molecular details of S100A11 and ANXA2 interaction during PMR, we used three S100A11 mutants; S100A11ΔCa lacking the Ca^{2+}-binding domain essential for Ca^{2+}-induced conformational changes and S100A11-ANXA2 interaction[37], S100A11ΔN lacking 23 amino acids at the NH_2- terminus essential for S100A11-ANXA2 interaction[36] and S100A11ΔC lacking 19 amino acids at the C-terminus, suggested to interact with actin[37]. We transfected HeLa cells with these S100A11 mutants tagged with GFP and monitored their injury-triggered trafficking and effects on the trafficking of RFP-tagged ANXA2 as well as wild type S100A11. Contrary to the wild type S100A11 (Fig. 4a-c), all three mutants failed to translocate to the injury site (Fig. 4f-h). In a dominant negative manner, S100A11ΔCa (Fig. 4f and Supplementary Figure 2e) and S100A11ΔN (Fig. 4g), but not S100A11ΔC (Fig. 4h), prevented the recruitment of ANXA2 (Fig. 4f-h) and wild type S100A11 (Supplementary Figure 2e) to the damaged membrane. To examine interaction between ANXA2 and S100A11 proteins we carried out Co-IP experiment using RFP antibody in HeLa cells co-expressing ANXA2-RFP and WT or mutant S100A11-GFP. Following scrape injury, anti-RFP antibody was able to co-IP ANXA2-RFP with wild type and ΔCa S100A11 mutant indicating the ability of ANXA2 to form a complex with these S100A11 proteins (Fig. 4i, upper panel). Further, IP with GFP antibody in MCF7-p95ErbB2 cells expressing ANXA2-GFP resulted in co-IP of endogenous S100A11 protein from these cells (Fig. 4i, lower panel). A characteristic feature of the S100 family of calcium-binding proteins is that they form non-covalent homodimers[18]. Thus the dominant negative effect of S100A11ΔCa and S100A11ΔN further suggests that S100A11 and ANXA2 are recruited to the injury site as a complex.

S100A11-ANXA2 complex augments PMR by altering local actin dynamics

In view of the ability of S100A11 to bind F-actin in a Ca^{2+}-dependent manner[38, 39] and of ANXA2 to regulate the formation and growth of F-actin bundles[12, 40] together with the need of F-actin assembly to control PMR in other organisms[9, 41], we tested whether S100A11 and ANXA2 regulate PMR by regulating actin dynamics in human cells. Our previous *in vitro* studies have identified that GST tagged S100A11 protein interacts with F-actin (not G-actin) in a dose dependent manner[38]. We carried out co-IP experiment by expressing S100A11-tGFP in HeLa cells and confirmed *in vivo* interaction of S100A11 with β-actin (Fig. 5a). In uninjured cells, S100A11 and β-actin distributed uniformly throughout the cells but glass bead-induced plasma membrane injury caused co-accumulation of β-actin and S100A11 at

the damaged membranes (Fig. 5b). Immediately following laser-induced plasma membrane injury and prior to the accumulation of S100A11, the level of β-actin at the site of injury decreased (Fig. 5c). This was followed by the accumulation of S100A11 and the subsequent buildup of β-actin (Fig. 5c, Supplementary Figure 3a, Supplementary Movie 5). Upon completion of PMR, both proteins returned back to their pre-injury distribution at the repair site.

To test if S100A11-ANXA2 complex regulates F-actin dynamics at the repair site we probed F-actin with utrophin-mCherry[42]. In HeLa cells, in the presence of endogenous S100A11, ANXA1 was rapidly recruited to the injured part of the plasma membrane (not shown) followed by localized F-actin buildup at the site of repair (Fig. 5d, Supplementary Movie 6). Depletion of S100A11 prevented F-actin accumulation completely. Instead, the level of F-actin around the injured membrane declined rapidly and the cell failed to repair the membrane (Fig. 5d and 5e). A similar S100A11-dependent increase in the level of utrophin-mCherry near the injured membrane was observed in MCF7-p95ErbB2 cells (Fig. 5e and Supplementary Figure 3b). Thus, S100A11-ANXA2 complex may regulate membrane repair by facilitating cortical actin polymerization beneath the injury site thereby assisting the closure of the wound.

Time-lapse imaging of the repair process in laser-injured cells revealed that S100A11 was recruited to the injury site in waves, each wave of S100A11 correlating with a subsequent increase in F-actin build-up (Fig. 6a, Supplementary Movie 7). This process was absent in cells expressing the dominant negative S100A11ΔCa mutant (Fig. 6b), which inhibited S100A11-ANXA2 complex recruitment to the injured membrane (Fig. 4f and Supplementary Figure 2e). Supporting the importance of actin dynamics in the repair process, inhibition of F-actin remodeling by either cytochalasin D (actin polymerization inhibitor) or jasplakinolide (actin depolymerization inhibitor) also significantly impaired PMR after local laser injury (Fig. 6c). This occurred to the extent that many drug-treated cells were severely damaged as illustrated by the accumulation of ANXA1-GFP to the large parts of the membrane (Fig. 6d). Altering F-actin dynamics by treatment with either cytochalasin D or jasplakinolide did not affect the ability of S100A11 (Fig. 6e) to accumulate at the site of injury. These proteins remained, however, at the site of injury 4-5 times longer than in untreated control cells (Fig. 6e and 6f). These findings suggest that accumulation of S100A11 and ANXA2 at the injured membrane is independent of F-actin dynamics, but normal F-actin assembly and disassembly are required for effective PMR and clearance of S100A11-ANXA2 complex from the membrane.

S100A11 is required for tumor cell invasiveness

As we have reported before[29], p95ErbB2 expression also provided MCF7 cells with a capacity to invade into 3-dimensional matrigel matrix, a process that exposes cell membranes to an even higher degree of physical stress. In view of our above findings that invasive phenotype triggered by p95ErbB2 overexpression is associated with increased need for PMR by S100A11 and ANXA2, we investigated if blocking S100A11-dependent PMR machinery would compromise the invasive phenotype. Unlike MCF7-p95ErbB2 cells transfected with control siRNA that migrated out of the matrigel matrix, S100A11-depleted

MCF7-p95ErbB2 cells resembled the MCF7-vector cells that formed non-invading compact spheroids (Fig. 7a). In view of the involvement of S100A11 in metastatic cell migration[21] we examined if reduced invasiveness of S100A11 depleted MCF7-p95ErbB2 cells reflects loss in cell mobility. We monitored motility of MCF7-p95ErB2 cells treated for 72 h with S100A11-specific or control siRNA and found no difference in mean cellular velocity of these cells (Fig. 7b). Additionally, unlike improved PMR of HeLa cells over expressing S100A11 (Fig. 2c), over expression of S100A11 did not enhance the motility of HeLa cells to migrate into and close a gap in a cell monolayer created by scratching of the cell monolayer (Fig. 7c). These findings suggest that despite normal cellular motility, poor PMR can restrict the invasive ability of MCF7-p95ErbB2 cells in 3-D matrigel matrix.

DISCUSSION

Our results demonstrate that MCF7 breast cancer cells made metastatic by ectopic expression of p95ErbB2 oncoprotein require enhanced PMR through increased expression of S100A11 and ANXA2 proteins. As a result of enhanced PMR these cells are more efficient than the non-invasive MCF7 cells at maintaining plasma membrane integrity following various stresses and injuries due to their invasive nature. Accordingly, loss of S100A11-ANXA2 complex reduces their viability and compromises their invasive ability. These observations indicate that repairing injured cell membranes is critical for survival and metastasis and thus explain the need for high S100A11 levels in metastatic cells of various origins[25-27].

ANXA1, a binding partner of S100A11, is recruited to the injured cell membrane in a Ca^{2+} dependent manner, presumably to initiate repair response[14]. However, the recruitment of ANXA1 at the site of injury is independent of S100A11 binding, as it persists in cells lacking S100A11. Moreover, ANXA1 accumulates at the damaged part of the cell that is eventually excised while S100A11 is recruited to the site where new cortical actin builds up and helps with the excision of the damaged cell membrane. Our data offer the first clear demonstration of such an excision process and provides the underlying mechanism regulating this process.

Unlike ANXA1 we find that ANXA2 co-localizes with S100A11 at the injury site and their presence at the repair site is mutually dependent. This is in line with the 5-fold tighter Ca^{2+}-dependent *in vitro* interaction of S100A11 with ANXA2 as compared with ANXA1[36]. Mutation in S100A11 that prevents its Ca^{2+} binding or deletions of either NH_2- or C-terminus inhibit the ability of S100A11 to localize to the site of injury and inhibit PMR. This is consistent with the requirements of S100A11 NH_2-terminal amino acids and Ca^{2+}-induced conformational change for S100A11-ANXA2 interaction[36, 38]. Our data demonstrates that the key function of S100A11-ANXA2 complex in PMR is to aid in remodeling of actin cytoskeleton at the site of injury to facilitate excision of the damaged cell membrane. This function of S100A11-ANXA2 complex is in agreement with work showing individual interactions of S100A11 and ANXA2 proteins with the actin cytoskeleton[12, 38]. The participation of actin in the cell membrane repair process has been shown to be important in Xenopus oocytes and Drosophila embryo[9, 10]. Thus, actin appears to be the evolutionarily conserved facilitator of cell membrane repair. While the

involvement of S100 in PMR has not been examined in these model systems, annexins have been shown to regulate PMR in zebrafish[43]. It is not known if annexin-mediated PMR in zebrafish involves modulation of actin cytoskeleton. Here we show that S100A11-ANXA2 complex interacts with β-actin and that it is required for the proper re-modeling of actin to facilitate wound closure in mammalian cells.

The important role of actin dynamics in this process is further supported by inhibition of PMR by drugs that block actin polymerization or de-polymerization[41]. We propose that this is due to the role of membrane-associated cortical actin cytoskeleton in maintaining cell membrane stability. While cortical F-actin is necessary to support the cell membrane, it also creates tension that would inhibit passive resealing after injury[7]. Thus, depolymerizing cortical actin after injury would not only keep the tension from further damaging the injured cell membrane, but will also facilitate membrane fusion to enhance the repair of the wounded membrane[44]. Localized wounding of 3T3 fibroblasts has been shown to significantly reduce membrane tension in a Ca^{2+}-dependent manner[7]. This could be due to the cortical actin depolymerization triggered by calcium-induced activation of F-actin severing proteins such as gelsolin[45]. Loss of tension and clearance of cortical actin together with increased cell membrane access for vesicles can contribute to the repair of the wounded membrane[44]. Based on our observations we have proposed a model that depicts the various steps during PMR (Fig. 7d). In resting cell ANXA1, ANXA2 and S100A11 are predominantly cytosolic and there is a layer of cortical actin under the cell membrane. Following cell membrane injury the cortical F-actin consistently decreases around the injury site concomitant with the recruitment of ANXA1 at the injured cell membrane. We propose that Ca^{2+}-triggered local loss of F-actin by actin severing proteins reduces membrane tension and brings together the wounded edges of the cell membrane (Fig 7d). This is followed by Ca^{2+}-dependent accumulation of S100A11-ANXA2 complex near the injury site. As S100A11 and ANXA2 bind F-actin and decrease the depolymerization rate of preformed actin filaments[12, 38], the S100A11-ANXA2 complex restricts F-actin depolymerization, preserving and allowing new buildup of F-actin around the injury site. ANXA2 is also capable of Ca^{2+}-dependent binding to phospholipids, which enables aggregation of endosomes and other vesicles[46]. At these membranes S100A11-ANXA2 complex helps nucleate polymerization of cortical F-actin by, enabling buildup of cortical F-actin[40]. The buildup of the cortical F-actin together with presence of vesicular endomembrane and the wounded edges of the plasma membrane all participate in the fusion of the wounded cell membrane at the repair site marked by S100A11-ANXA2 complex and the excision of the damaged part of the cell membrane marked by ANXA1. The buildup of cortical actin we observe here is analogous to F-actin drawstring formation during healing of injured Xenopus oocyte cell membrane[9]. Thus, we propose that the F-actin buildup allows pulling the wounded membrane edges together during excision to facilitate repair. Recently, it has been shown that Ca^{2+}-regulated cyclic assembly and disassembly of F-actin at the cell membrane regulates vesicle fusion[47]. Thus the vesicle aggregation and F-actin assembly mediated by the S100A11-ANXA2 complex may help with PMR by facilitating vesicle fusion and cortical actin buildup. Lysosomes are among the vesicles whose Ca^{2+}-triggered fusion has been linked to PMR[5]. Accordingly, Ca^{2+} influx caused by injury or ionomycin resulted in an increase in lysosome exocytosis. However, extent of lysosomal exocytosis is

unaltered by S100A11 expression. S100A11 depletion does result in increased basal lysosomal exocytosis, but this is likely due to the poor repair following spontaneous plasma membrane damage in S100A11 depleted cells. While S100A11-ANXA2 complex does not regulate lysosome exocytosis in response to injury it remains plausible that this complex regulates the fusion of other vesicles involved in PMR[35].

S100A11 localized to nucleus has been shown to inhibit keratinocyte growth liberating Sp1/3 from nucleolin to activate the negative cell cycle regulator $p21^{CIP1/WAF1}$, whereas secreted S100A11 can activate cell growth[37, 48]. To this end, our results identify that maintaining plasma membrane integrity is a key intracellular function of S100A11 in the metastatic cells. This functional duality of S100A11 may benefit by linking large membrane injury to G1 cell cycle arrest thus keeping injured cells from entering cell division until they have successfully recovered. Our finding of a role of S100A11 in regulating cell membrane and associated cytoskeleton adds to a recent study of six metastatic cancer cell lines, that reported significant reduction in pseudopod formation and invasion after S100A11 knock down[21]. It is interesting to note that all of these processes are dependent on the function of the actomyosin complex, defects in which we have found to be responsible for the poor PMR in these cells.

In summary, our study demonstrates that metastatic cancer cells have elevated rate of cell injury and that they rely on S100A11-ANXA2 complex to enable cell membrane repair. The repair response proceeds by excision of the damaged part of the cell membrane. Our findings suggest that S100A11-ANXA2 complex, injury triggered actin remodeling and other steps in the plasma membrane repair response are novel and viable targets for controlling tumor cell metastasis.

METHODS

Cell culture and treatments

MCF7 and HeLa cells originate from human breast carcinoma and cervix carcinoma respectively and were obtained from ATCC. MCF7-p95ErbB2 and MCF7-pTRE cell lines are single cell clones of MCF-7 expressing the tetracycline transactivator transfected with pTRE-p95ErbB2 and pTRE, respectively [32]. To induce p95ErbB2 expression, tetracycline (1 μg/ml) was removed and cells were washed 5 times in PBS before plating.

siRNAs and plasmid constructs

For all siRNAs knockdown 20nM siRNA was used. Sequence of the siRNAs used is listed in Table 1. Control siRNA: AllStar Negative Control siRNA (QIAGEN). Plasmids: Human S100A11-turboGFP/S100A11-turboRFP with C-terminal GFP tag were purchased from OriGene Technologies. ANXA1-GFP was kindly obtained from[49], ANXA2-GFP/RFP from Arun Deora[50], Utrophin-mCherry from William Bement[42]. The S100A11 deletion mutants were similar to before[37] and constructed as GFP fusions in the manner described below. To eliminate Ca^{2+}-binding capacity, by site-directed mutagenesis amino acids 38E in the loop 1 and 72D, 76D, and 79E in the loop 2 were changed to S (S100A11ΔCa). For S100A11ΔN, human S100A11 cDNA lacking 23 amino acids from the N-terminus and for S100A11ΔC,

human S100A11 cDNA lacking 19 amino acids from C-terminus were obtained by PCR and the DNA sequence confirmed. The full length (WT), mutant and deletion cDNA constructs of S100A11 were inserted into the pDNR-1r (CMV-CMV) vector to express the constructs as N-terminal enhanced green fluorescent protein (EGFP) fusion proteins.

Immunoblot analysis, immunocytochemistry and immunoprecipitation

Proteins were separated by SDS-PAGE and transferred to nitrocellulose membranes. Primary antibodies raised against human S100A11 (1:1000 dilution) (ProteinTech Group), Annexin A1 (1:1000 dilution) (Abcam), Annexin A2 (1:1000 dilution) (BD Transduction Laboratories), heat shock cognate 70 kDa protein (1:6000 dilution) (Hsc70; N69, kindly provided by Boris Margulis, Russian Academy of Sciences, St. Petersburg, Russia), α-tubulin (1:5000) (Abcam) and ErbB2 (1:1000) (Fischer Thermo Scientific, MA) was used. This was followed by appropriate peroxidase-conjugated secondary antibodies (DAKO). Immunocytochemistry: cells on coverslips were fixed in paraformaldehyde and stained with indicated primary antibodies (1:300 dilution) including S100A11 and β-actin (Sigma). Samples were incubated with the appropriate Alexa Fluor-488– and Alexa- Fluor-546/594-coupled secondary antibodies (1:1000 dilution) (Molecular Probes) and images taken by confocal microscopy. Immunoprecipitation (IP) was performed on lysates from HeLa or MCF7-ErbB2 cells overexpressing ANXA2-RFP and S100A11-GFP (wild type or mutants) or only S100A11-turbo-GFP. Immuno complexes were captured with RFP-Trap agarose beads (Chromotek) or turbo-GFP antibody (OriGene) coupled to sepharose-G beads and washed 4 times before immunoblot analysis (Extended blots showing Co-IP are presented in Supplementary Figure 4).

RNA extraction and qPCR

Total RNA was isolated with the NucleoSpin Total RNA Isolation Kit (Macherey-Nagel, Germany) and complementary DNA was synthesized with the TaqMan Reverse Transcription Kit (Roche) according to the manufacturers' protocols. The primers used for qPCR are listed in Table 2.

Membrane integrity and cytometry

Analysis of LAMP1 membrane levels: cells were incubated with anti-LAMP1 (Santa Cruz Biotechnology) antibody on ice for 30 min, fixed by paraformaldehyde and stained with Alexa Fluor 488 antibody. Plasma membrane integrity +/− scrape injury was performed by incubating cells (after injury) with impermeant 7-aminoactinomycin D (*7-AAD*) for 10 min followed by flow cytometry with a FACS (Becton Dickinson, CELLQUEST software). To measure membrane integrity, cells seeded in chamber slides were incubated with impermeant Hoechst-3342 in imaging media (Hanks Balanced Salt Solution with 10 mM HEPES and 1% FCS, pH 7.4) +/− 2 mM Ca^{2+}. Hoechst-3342 uptake was imaged by a Carl Zeiss Axiovert 200M fluorescence time-lapse microscope and analyzed using MetaMorph software. Cell death by PI exclusion assay was measured with an image based Celigo cytometer (Brooks) according to manufacturer's instructions.

Membrane wounding experiments

These experiments were performed as detailed elsewhere[34, 35] and described here briefly. Glass bead injury: Cells were injured by rolling glass beads (425-600 μm, acid washed. Sigma) in cell imaging media (CIM − HBSS + 10mM Hepes + 2mMCa^{2+} pH 7.4) containing 2 mg/mL lysine fixable 10-kDa FITC dextran. After healing at 37 °C for 5 min cells were transferred to CIM containing 2 mg/mL lysine fixable 10-kDa Tetramethyl Rhodamine Isothicyanate (TRITC)-dextran for another 5 minutes. After paraformaldehyde fixation the number of FITC-positive (total wounded cells) and TRITC-positive cells (wounded cells which have not resealed) were counted. Laser injury: Cells were injured in CIM with 1 μg/μl of FM1-43 dye by selecting a small region (1-5 μm^2) and irradiating with a pulsed laser (AblateTM). Cells were imaged every 10 seconds starting prior to injury and continuing for 3-5 minutes following injury. For no repair control, cells were injured in Ca^{2+} free PBS containing 1 μg/μL of FM dye. The hardware were controlled using Slidebook 5.0 (Intelligent Imaging Innovations Inc., Denver) and the same software was used to measure the kinetics of repair by monitoring cellular FM dye fluorescence as change in intensity (ΔF/F0) during the course of imaging.

3D matrigel invasion assay

Cells were incubated overnight to form spontaneous spheroids on an inverted lid in a hanging drop containing $2{,}5\times10^5$ cells in RPMI tissue culture media (TCM) (GIBCO) with 10% FCS (GIBCO). The day after the spheroids were transferred to a layer of polymerized Matrigel (growth factor reduced; Becton Dickenson) diluted 1:1 with TCM. The spheroids were covered with a sealing layer of Matrigel mix and the TCM was added to cover the cells. The extent of the outgrowth was carefully followed up to 4 days. Images were taken with Olympus 1X71 light microscope supplemented with Cella P software.

Supplementary Material

Refer to Web version on PubMed Central for supplementary material.

ACKNOWLEDGEMENTS

We thank K. Grøn Henriksen for excellent technical assistance. We thank Drs. Arun Deora and Kathy Hajjar (Weill Medical College of Cornell University, NY) for Annexin A2 constructs and Dr. William Bement (University of Wisconsin-Madison) for Utrophin-mCherry construct. We thank all members of the Jaiswal lab and Unit for Cell Death and Metabolism for their helpful comments as well as assistance in carrying out this work. This work was supported by National Institutes of Health Grants R01AR055686, P50AR060836, and P30HD040677 (J.K.J.), Danish Medical Research Council (J.N. and M.J.), Danish Cancer Society (M.J.), Lundbeck Foundation (M.J.), Novo Nordisk Foundation (M.J.) and Association for International Cancer Research (M.J.).

REFERENCES

1. Bansal D, et al. Defective membrane repair in dysferlin-deficient muscular dystrophy. Nature. 2003; 423:168–172. [PubMed: 12736685]
2. Howard AC, McNeil AK, Xiong F, Xiong WC, McNeil PL. A novel cellular defect in diabetes: membrane repair failure. Diabetes. 2011; 60:3034–3043. [PubMed: 21940783]
3. Huynh C, Roth D, Ward DM, Kaplan J, Andrews NW. Defective lysosomal exocytosis and plasma membrane repair in Chediak-Higashi/beige cells. Proc. Natl. Acad. Sci. U. S. A. 2004; 101:16795–16800. [PubMed: 15557559]

4. Draeger A, Monastyrskaya K, Babiychuk EB. Plasma membrane repair and cellular damage control: the annexin survival kit. Biochem. Pharmacol. 2011; 81:703–712. [PubMed: 21219882]
5. Reddy A, Caler EV, Andrews NW. Plasma membrane repair is mediated by Ca(2+)-regulated exocytosis of lysosomes. Cell. 2001; 106:157–169. [PubMed: 11511344]
6. McNeil PL, Vogel SS, Miyake K, Terasaki M. Patching plasma membrane disruptions with cytoplasmic membrane. J. Cell Sci. 2000; 113(Pt 11):1891–1902. [PubMed: 10806100]
7. Togo T, Krasieva TB, Steinhardt RA. A decrease in membrane tension precedes successful cell-membrane repair. Mol. Biol. Cell. 2000; 11:4339–4346. [PubMed: 11102527]
8. Abreu-Blanco MT, Verboon JM, Parkhurst SM. Single cell wound repair: Dealing with life's little traumas. Bioarchitecture. 2011; 1:114–121. [PubMed: 21922041]
9. Bement WM, Mandato CA, Kirsch MN. Wound-induced assembly and closure of an actomyosin purse string in Xenopus oocytes. Curr. Biol. 1999; 9:579–587. [PubMed: 10359696]
10. Abreu-Blanco MT, Verboon JM, Parkhurst SM. Cell wound repair in Drosophila occurs through three distinct phases of membrane and cytoskeletal remodeling. J. Cell Biol. 2011; 193:455–464. [PubMed: 21518790]
11. Grieve AG, Moss SE, Hayes MJ. Annexin A2 at the interface of actin and membrane dynamics: a focus on its roles in endocytosis and cell polarization. Int. J. Cell Biol. 2012; 2012:852430. [PubMed: 22505935]
12. Hayes MJ, Shao D, Bailly M, Moss SE. Regulation of actin dynamics by annexin 2. EMBO J. 2006; 25:1816–1826. [PubMed: 16601677]
13. Bouter A, et al. Annexin-A5 assembled into two-dimensional arrays promotes cell membrane repair. Nat. Commun. 2011; 2:270. [PubMed: 21468022]
14. McNeil AK, Rescher U, Gerke V, McNeil PL. Requirement for annexin A1 in plasma membrane repair. J. Biol. Chem. 2006; 281:35202–35207. [PubMed: 16984915]
15. Potez S, et al. Tailored protection against plasmalemmal injury by annexins with different Ca2+ sensitivities. J. Biol. Chem. 2011; 286:17982–17991. [PubMed: 21454475]
16. Lennon NJ, et al. Dysferlin interacts with annexins A1 and A2 and mediates sarcolemmal wound-healing. J. Biol. Chem. 2003; 278:50466–50473. [PubMed: 14506282]
17. Scharf B, et al. Annexin A2 binds to endosomes following organelle destabilization by particulate wear debris. Nat. Commun. 2012; 3:755. [PubMed: 22453828]
18. Rintala-Dempsey AC, Rezvanpour A, Shaw GS. S100-annexin complexes--structural insights. FEBS J. 2008; 275:4956–4966. [PubMed: 18795951]
19. Gerke V, Moss SE. Annexins: from structure to function. Physiol Rev. 2002; 82:331–371. [PubMed: 11917092]
20. Swaminathan V, et al. Mechanical stiffness grades metastatic potential in patient tumor cells and in cancer cell lines. Cancer Res. 2011; 71:5075–5080. [PubMed: 21642375]
21. Shankar J, et al. Pseudopodial actin dynamics control epithelial-mesenchymal transition in metastatic cancer cells. Cancer Res. 2010; 70:3780–3790. [PubMed: 20388789]
22. Melle C, et al. Different expression of calgizzarin (S100A11) in normal colonic epithelium, adenoma and colorectal carcinoma. Int. J. Oncol. 2006; 28:195–200. [PubMed: 16327996]
23. Cross SS, Hamdy FC, Deloulme JC, Rehman I. Expression of S100 proteins in normal human tissues and common cancers using tissue microarrays: S100A6, S100A8, S100A9 and S100A11 are all overexpressed in common cancers. Histopathology. 2005; 46:256–269. [PubMed: 15720411]
24. Rehman I, et al. Dysregulated expression of S100A11 (calgizzarin) in prostate cancer and precursor lesions. Hum. Pathol. 2004; 35:1385–1391. [PubMed: 15668896]
25. Xiao MB, et al. High expression of S100A11 in pancreatic adenocarcinoma is an unfavorable prognostic marker. Med. Oncol. 2012; 29:1886–1891. [PubMed: 21912994]
26. Tian T, et al. Determination of metastasis-associated proteins in non-small cell lung cancer by comparative proteomic analysis. Cancer Sci. 2007; 98:1265–1274. [PubMed: 17537172]
27. Melle C, Ernst G, Schimmel B, Bleul A, Von EF. Colon-derived liver metastasis, colorectal carcinoma, and hepatocellular carcinoma can be discriminated by the Ca(2+)-binding proteins S100A6 and S100A11. PLoS. One. 2008; 3:e3767. [PubMed: 19048101]

28. Nylandsted J, et al. ErbB2-associated changes in the lysosomal proteome. Proteomics. 2011; 11:2830–2838. [PubMed: 21674799]
29. Rafn B, et al. ErbB2-driven breast cancer cell invasion depends on a complex signaling network activating myeloid zinc finger-1-dependent cathepsin B expression. Mol. Cell. 2012; 45:764–776. [PubMed: 22464443]
30. Martin M, et al. ERBB2 overexpression triggers transient high mechanoactivity of breast tumor cells. Cytoskeleton. 2012; 69:267–277. [PubMed: 22407943]
31. Cardoso CM, et al. Depletion of kinesin 5B affects lysosomal distribution and stability and induces peri-nuclear accumulation of autophagosomes in cancer cells. PLoS. One. 2009; 4:e4424. [PubMed: 19242560]
32. Egeblad M, Mortensen OH, Jaattela M. Truncated ErbB2 receptor enhances ErbB1 signaling and induces reversible, ERK-independent loss of epithelial morphology. Int. J. Cancer. 2001; 94:185–191. [PubMed: 11668496]
33. Babiychuk EB, Monastyrskaya K, Potez S, Draeger A. Blebbing confers resistance against cell lysis. Cell Death. Differ. 2011; 18:80–89. [PubMed: 20596076]
34. Defour A, Senchandra S, Jaiswal JK. Imaging cell membrane injury and sub-cellular processes involved in repair. J Vis Exp. 2014; (85):e51106. doi:10.3791/51106.
35. Jaiswal JK, et al. Patients with a non-dysferlin Miyoshi myopathy have a novel membrane repair defect. Traffic. 2007; 8:77–88. [PubMed: 17132147]
36. Rintala-Dempsey AC, Santamaria-Kisiel L, Liao Y, Lajoie G, Shaw GS. Insights into S100 target specificity examined by a new interaction between S100A11 and annexin A2. Biochemistry. 2006; 45:14695–14705. [PubMed: 17144662]
37. Sakaguchi M, et al. S100C/A11 is a key mediator of Ca(2+)-induced growth inhibition of human epidermal keratinocytes. J. Cell Biol. 2003; 163:825–835. [PubMed: 14623863]
38. Sakaguchi M, et al. Relationship between contact inhibition and intranuclear S100C of normal human fibroblasts. J. Cell Biol. 2000; 149:1193–1206. [PubMed: 10851017]
39. Zhao XQ, Naka M, Muneyuki M, Tanaka T. Ca(2+)-dependent inhibition of actin-activated myosin ATPase activity by S100C (S100A11), a novel member of the S100 protein family. Biochem. Biophys. Res. Commun. 2000; 267:77–79. [PubMed: 10623577]
40. Morel E, Parton RG, Gruenberg J. Annexin A2-dependent polymerization of actin mediates endosome biogenesis. Dev. Cell. 2009; 16:445–457. [PubMed: 19289089]
41. Burkel BM, Benink HA, Vaughan EM, von Dassow G, Bement WM. A Rho GTPase signal treadmill backs a contractile array. Dev. Cell. 2012; 23:384–396. [PubMed: 22819338]
42. Burkel BM, von Dassow G, Bement WM. Versatile fluorescent probes for actin filaments based on the actin-binding domain of utrophin. Cell Motil. Cytoskeleton. 2007; 64:822–832. [PubMed: 17685442]
43. Roostalu U, Strahle U. In vivo imaging of molecular interactions at damaged sarcolemma. Dev. Cell. 2012; 22:515–529. [PubMed: 22421042]
44. Miyake K, McNeil PL, Suzuki K, Tsunoda R, Sugai N. An actin barrier to resealing. J. Cell Sci. 2001; 114:3487–3494. [PubMed: 11682608]
45. Yin HL, Iida K, Janmey PA. Identification of a polyphosphoinositide-modulated domain in gelsolin which binds to the sides of actin filaments. J. Cell Biol. 1988; 106:805–812. [PubMed: 2831234]
46. Glenney JR Jr. Tack B, Powell MA. Calpactins: two distinct Ca++-regulated phospholipid- and actin-binding proteins isolated from lung and placenta. J. Cell Biol. 1987; 104:503–511. [PubMed: 2950118]
47. Wollman R, Meyer T. Coordinated oscillations in cortical actin and Ca2+ correlate with cycles of vesicle secretion. Nat. Cell Biol. 2012; 14:1261–1269. [PubMed: 23143397]
48. Sakaguchi M, et al. S100A11, an dual mediator for growth regulation of human keratinocytes. Mol. Biol. Cell. 2008; 19:78–85. [PubMed: 17978094]
49. Monastyrskaya K, Babiychuk EB, Hostettler A, Rescher U, Draeger A. Annexins as intracellular calcium sensors. Cell Calcium. 2007; 41:207–219. [PubMed: 16914198]

50. Deora AB, Kreitzer G, Jacovina AT, Hajjar KA. An annexin 2 phosphorylation switch mediates p11-dependent translocation of annexin 2 to the cell surface. J. Biol. Chem. 2004; 279:43411–43418. [PubMed: 15302870]

Europe PMC Funders Author Manuscripts

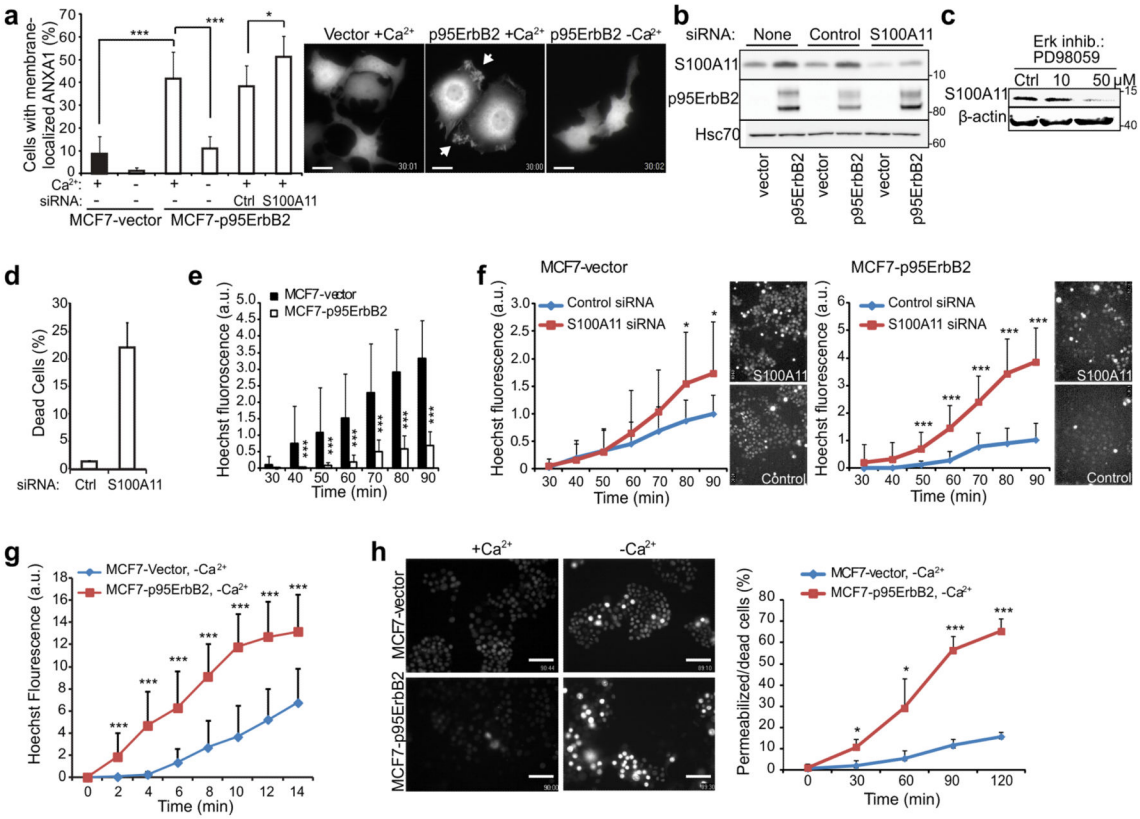

Figure 1. S100A11 protects MCF7 cells against p95ErbB2 expression-induced membrane damage

(a) Quantification (*left*) and representative images (*right*; scale bars, 20 μm) of ANXA1-GFP-expressing MCF7-vector and -p95ErbB2 cells with membrane associated ANXA1-GFP after 2 h incubation in medium with or without Ca^{2+}. When indicated, cells were transfected with control or S100A11-I siRNA 72 h prior to the experiment. See Supplementary Movie 1 for the dynamic distribution of ANXA1-GFP in MCF7-p95ErbB2 cells.

(b) Representative immunoblot of S100A11 (13 kDa), p95ErbB2 (95 kDa) and Hsc70 (70 kDa; loading control) in lysates of MCF7-vector and –p95ErbB2 cells left untreated or transfected with indicated siRNAs for 72 h. Markers listed represent protein molecular weights in KDa.

(c) Immunoblot of S100A11 level in MCF7-p95ErbB2 cells treated for 72 h with Erk inhibitor PD98059. β-actin served as loading control.

(d) Cell death assay in MCF7-p95ErbB2 cells 96 h after transfection with control or S100A11-I siRNA as analyzed by Propidium iodide (PI) exclusion assay and measured by using a fluorescence Celigo imaging cytometer.

(e) Permeability of MCF7-vector and -p95ErbB2 cells to Hoechst-3342 under normal growth conditions (30-90 min). Representative images of cells are shown in figure 1H ($+Ca^{2+}$ panel).

Europe PMC Funders Author Manuscripts

Europe PMC Funders Author Manuscripts

(f) Hoechst-3342 leakage into MCF7-vector and -p95ErbB2 cells treated with indicated siRNAs for 48 h. Fluorescence intensity in each replicate was normalized to that in control siRNA-treated cells 90 min after dye addition. Accompanying images were taken at 90 min.
(g) Influx of Hoechst-3342 into MCF7-p95ErbB2 and MCF7-vector cells incubated in Ca^{2+} free medium as measured every 2 minutes starting from the time the dye was added to the cells.
(h) Representative images of MCF7-vector and -p95ErbB2 cells incubated with Hoechst-3342 in imaging medium +/− Ca^{2+} for 120 min (*left*; scale bars, 100 μm) and quantification of permeabilized/dead cells at indicated time points (*right*).
Error bars, SD for a minimum of 20 randomly chosen cells / sample in a representative ($n \geq 3$) experiment (A, and F-H) or for three independent experiments in triplicate (D). Dead cells with high intensity staining were excluded from analysis in figures F-H. All data are representative of a minimum of three independent experiments. The asterisks represent *P* Values based on Students t-test: *P* Value: * $P < 0.05$, *** $P < 0.001$.

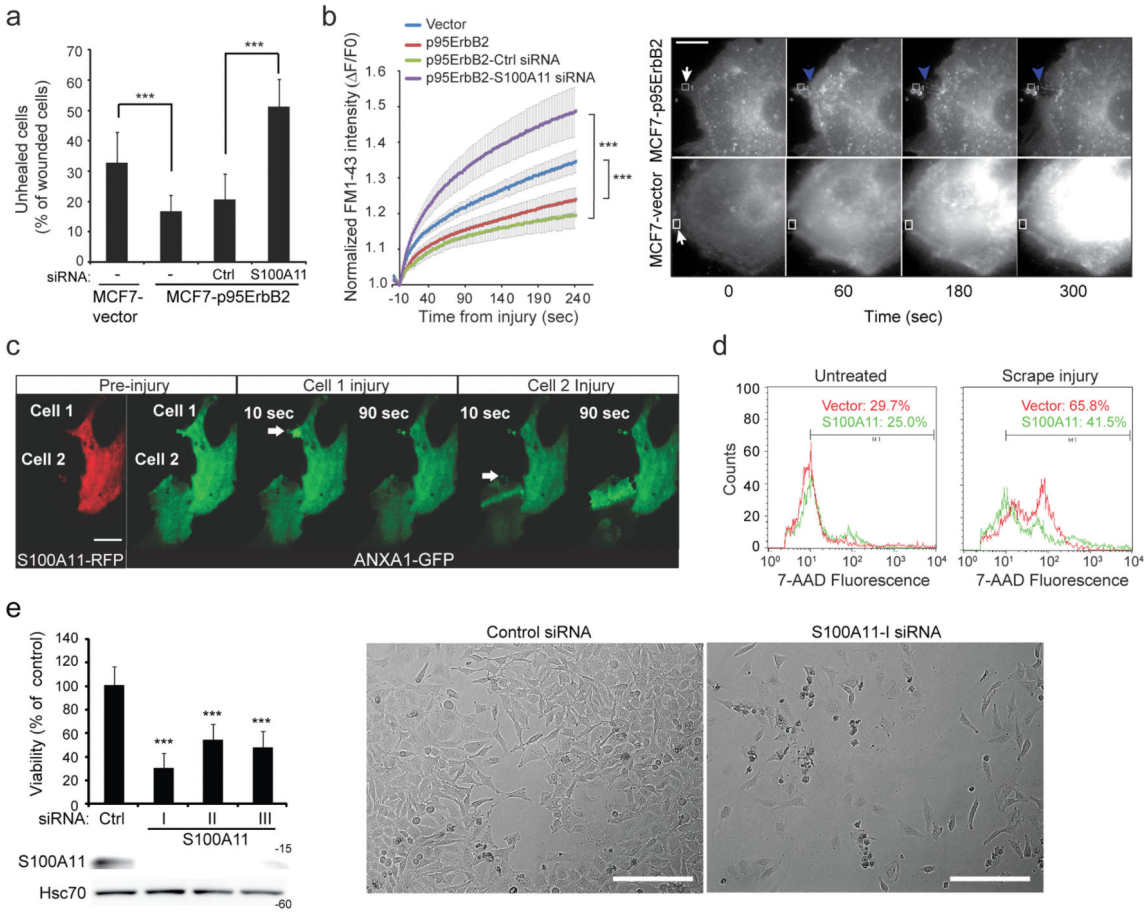

Figure 2. S100A11 improves repair of large plasma membrane injuries

(a) Quantification of MCF7-vector and -p95ErbB2 cells that failed to heal (TRITC-positive), 5 minutes following glass bead injury in the presence of FITC-dextran (labels all injured cells). When indicated, cells used were transfected for 72 h with indicated siRNAs. Error bars, SD for a triplicate representative (n = 3) experiment with 50-100 randomly chosen wounded cells / condition analyzed.

(b) Kinetics of cell membrane repair following laser injury. MCF7-vector and -p95ErbB2 cells incubated with FM1-43 dye were injured similarly by laser and the entry of FM1-43 was monitored by measuring FM1-43 intensity following injury (*left*). Error bars, SD for 10 independent cells / condition. Right panel shows representative images of cells before and after localized laser injury (white arrows). Note that unlike MCF7-vector cell, upon injury in MCF7-p95ErbB2 cell the damaged plasma membrane is excised and repaired at a new site marked by blue arrow.

(c) Images showing HeLa cells expressing S100A11-RFP and ANXA1-GFP (cell 1) or only ANXA1-GFP (cell 2) before and after localized laser injury (white arrows). Unlike cell 2 that does not overexpress S100A11, cell 1 repairs efficiently as indicated by the rapid clearance of ANXA1-GFP from the injury site; also see Video S2. Scale bar, 20 μm.

(d) FACS analysis of 7-AAD entry into uninjured and scrape injured HeLa cells allowed to repair for 10 minutes. Values indicate the percentage of cells in the gated area. The results are representative of three independent experiments.

Europe PMC Funders Author Manuscripts

(e) Viability of HeLa cells was analyzed by MTT reduction assay 96 h after transfection with control or S100A11 siRNAs (*top left)*. Error bars, SD for three independent experiments.

Representative immunoblots of S100A11 (13 kDa) and Hsc70 (70 kDa; loading control) in lysates of HeLa cells transfected with indicated siRNAs 72 h prior to the lysis (*bottom left)*. Representative phase contrast images of cells 96 h after transfection with indicated siRNAs (*right)*. Scale bar 1mm. The asterisks represent *P* Values based on Students t-test: *** $P <$ 0,001 when compared as indicated (A and B) or to the control siRNA-treated cells (E).

Europe PMC Funders Author Manuscripts

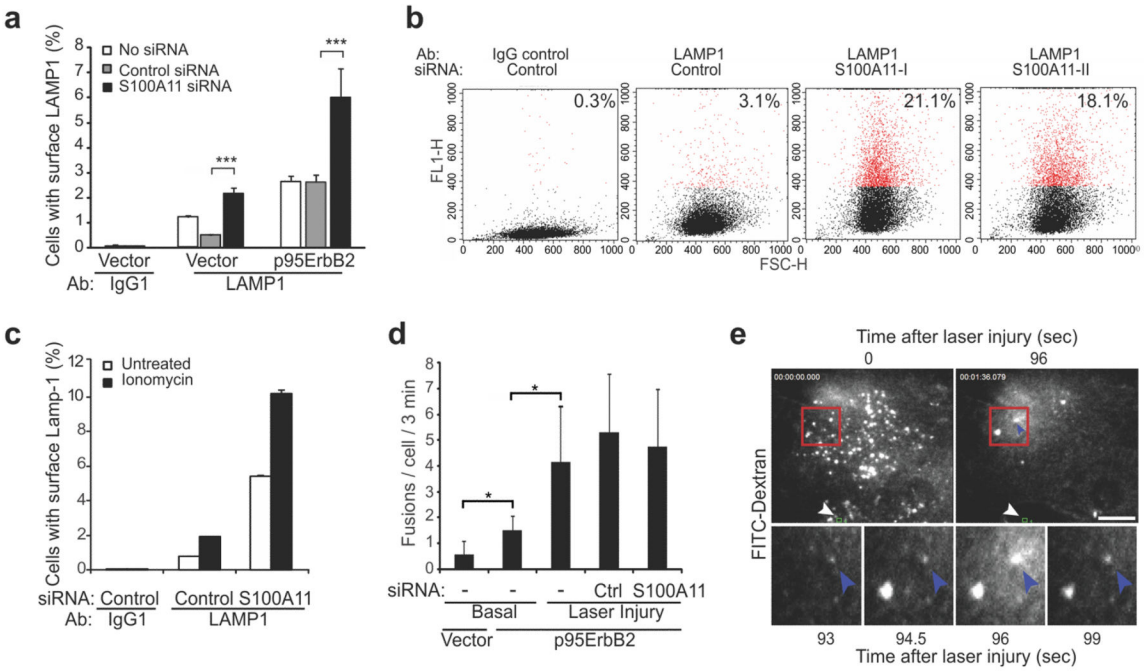

Figure 3. S100A11 increases basal but does not alter injury-dependent lysosomal exocytosis

(a) Quantification of LAMP1 surface staining in MCF7-vector and -p95ErbB2 cells by FACS. When indicated, cells were transfected with appropriate siRNA 72 h prior to the experiment. Error bars, SD for three independent experiments with 10000 cells / sample.

(b) Representative FACS profiles showing cell surface LAMP1 level (Y-axis) and cell count (X-axis) for HeLa cells transfected with control or S100A11-I siRNAs 72 h prior to the experiment. Red dots indicate M1-gated (cell surface LAMP1 positive) cells. Their percentage is indicated at the top right corner of each plot. See Fig. 2e for S100A11 knockdown and Supplementary Figure 1 for LAMP1 staining.

(c) Quantification of ionomycin-triggered increase in cell surface LAMP1 levels in HeLa cells. Cells were transfected with control or S100A11-I siRNAs 72 h prior to the experiment and then stained for cell surface LAMP1 prior to or following treatment with 10 μM ionomycin for 15 min. Error bars, SD for 10000 cells analyzed in a representative experiment.

(d) Laser injury-triggered exocytosis by FITC dextran-labeled lysosomes analyzed by TIRF microscopy. Exocytic fusions (flashes of FITC-dextran release) were counted for 3 minutes in uninjured cells (basal) and for 3 minutes following laser injury. Error bars, SD for 3 independent experiments with 5-10 cells / sample analyzed.

(e) TIRF images of FITC-dextran labeled lysosomes in a cell prior to (0 sec) and following (96 s) laser injury (*top*) as well as zoomed in frames from top panel showing a fusing lysosome (*bottom*). White arrow: site of injury; blue arrow lysosomal exocytic flash. The asterisks represent *P* Values based on Students t-test: * $P < 0{,}05$; *** $P < 0{,}001$.

Europe PMC Funders Author Manuscripts

Europe PMC Funders Author Manuscripts

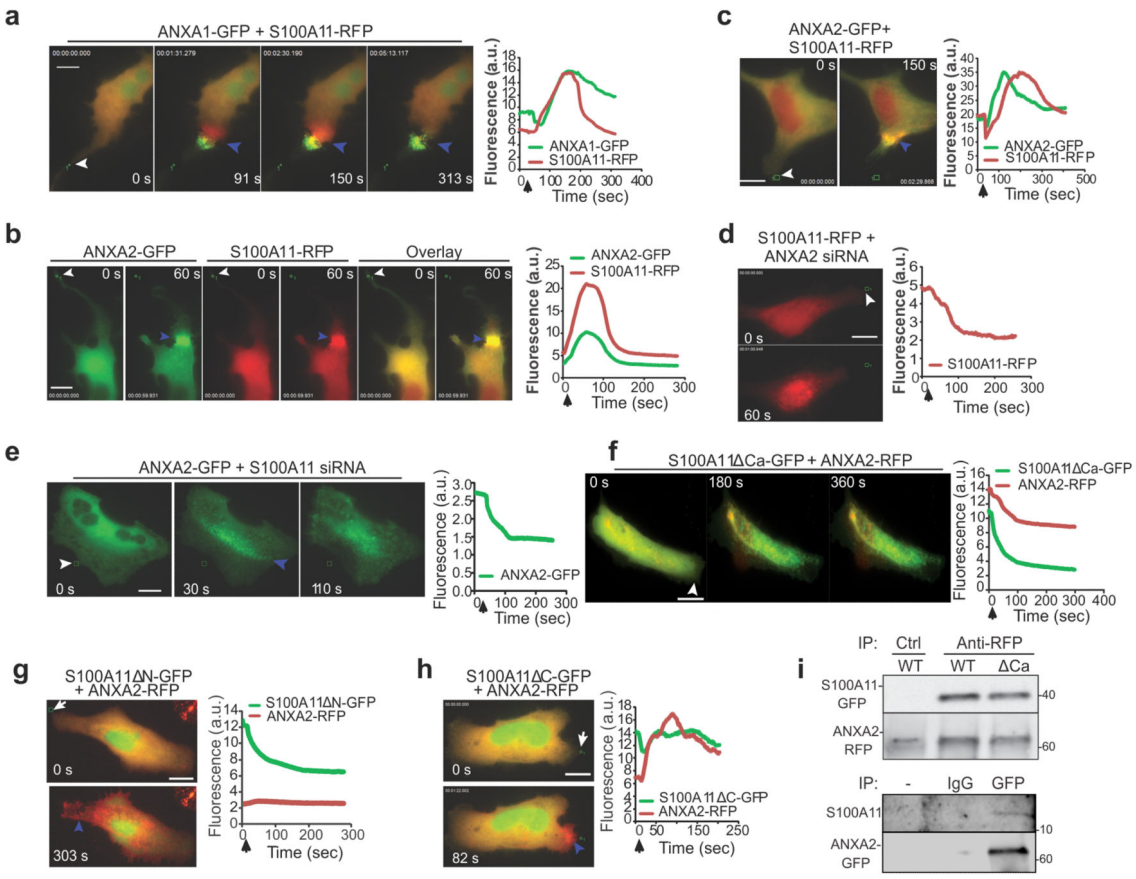

Figure 4. S100A11 forms a complex with ANXA2 and co-operate at the site of plasma membrane repair

(a) Images and plots showing the kinetics and localization of fluorescently-tagged S100A11 and ANXA1 in response to laser injury (white arrows: site of injury) in MCF7-p95ErbB2. (b, c) Images and plots showing the kinetics of accumulation of S100A11-RFP and ANXA2-GFP following laser injury in (b) MCF7-p95ErbB2 cells and (c) HeLa cells. Site of repair are indicated by blue arrows. (d) S100A11-RFP and (e) ANXA2-GFP accumulation at the site of injury (white arrowhead) monitored in HeLa cells 48 hours after silencing the expression of ANXA2 and S100A11 respectively. (f-h) HeLa cells expressing ANXA2-RFP and different S100A11 mutant proteins including (f) S100A11ΔCa-GFP, (g) S100A11ΔN-GFP or (h) S100A11ΔC-GFP were injured by laser (Injury site: white arrow) and imaged by timelapse microscopy. Results are representative of at least 5 experiments. Wherever indicated, blue arrowheads mark the site of repair and all scale bars represent 20 μm. (i) Representative co-immunoprecipitation using RFP or control antibodies from lysates of HeLa cells expressing ANXA2-RFP and S100A11-GFP and exposed to scrape injury (wild type/mutant). The panel below shows Western blot analysis of endogenous S100A11 co-IP using GFP antibody to pull down ANXA2-GFP from lysate of MCF7-p95ErbB2 cells expressing only ANXA2-GFP. This lysate was split into three parts and incubated with no antibody (−) Mouse IgG2 (IgG) or anti-GFP monoclonal antibody (GFP). Following IP Western blot analysis was carried out using S100A11 antibody.

Europe PMC Funders Author Manuscripts

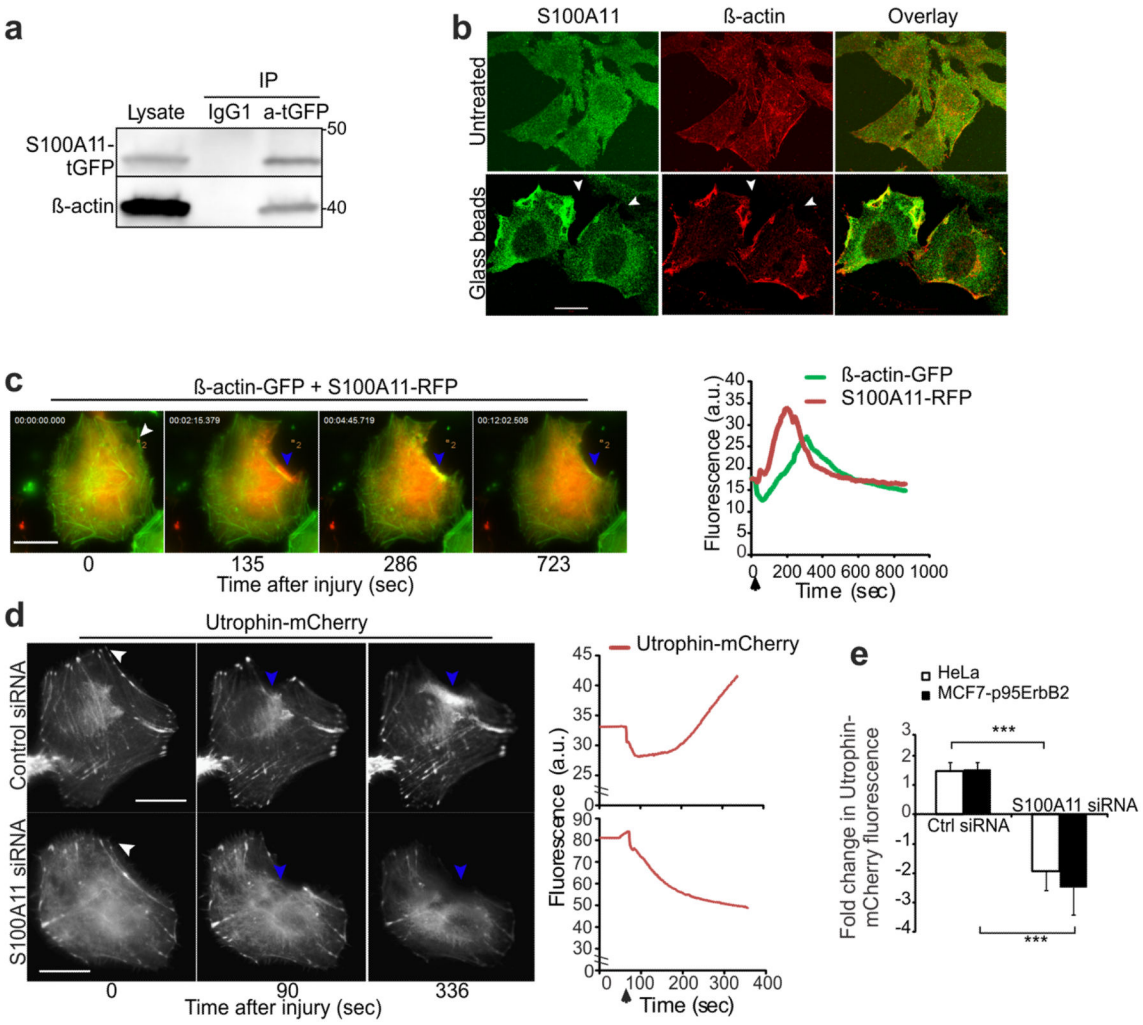

Figure 5. S100A11 is required for F-actin buildup at the site of plasma membrane repair

(a) Representative immunoblots of lysates of HeLa cells expressing S100A11-tGFP before or after immuno-precipitation using anti-tGFP or control IgG1 antibody and probed with S100A11 as well as β-actin antibodies.

(b) Images of HeLa cells stained for endogenous S100A11 and β-actin after glass bead injury. Co-localization of the two proteins at the damaged membrane is indicated by arrowheads.

(c) Images (*left*) of S100A11-RFP and β-actin-GFP recruitment to the repair site (blue arrowheads) in a HeLa cell following a local laser injury (white arrow). Corresponding plot (*right*) shows change in fluorescence intensity of these two proteins at the site of repair (blue arrowheads). Fig. S3A shows the images of individual channels and Video S5 shows the dynamics of this process.

(d) HeLa cells expressing endogenous S100A11 or knocked down for S100A11 were transfected with Utrophin-mCherry and its accumulation at the site of repair (blue arrow) was imaged (*left panel* and Video S6) and quantified (*right*) at the repair site in live cells.

(e) Average fold change in Utrophin-mCherry fluorescence around the repair site in HeLa and MCF7-p95ErbB2 cells respectively was quantified in each case for 5-7 cells, black arrows marks the time of injury. Also see Figure S3B. *** $P < 0{,}001$. Scale bar: 20 μm.

Europe PMC Funders Author Manuscripts

Europe PMC Funders Author Manuscripts

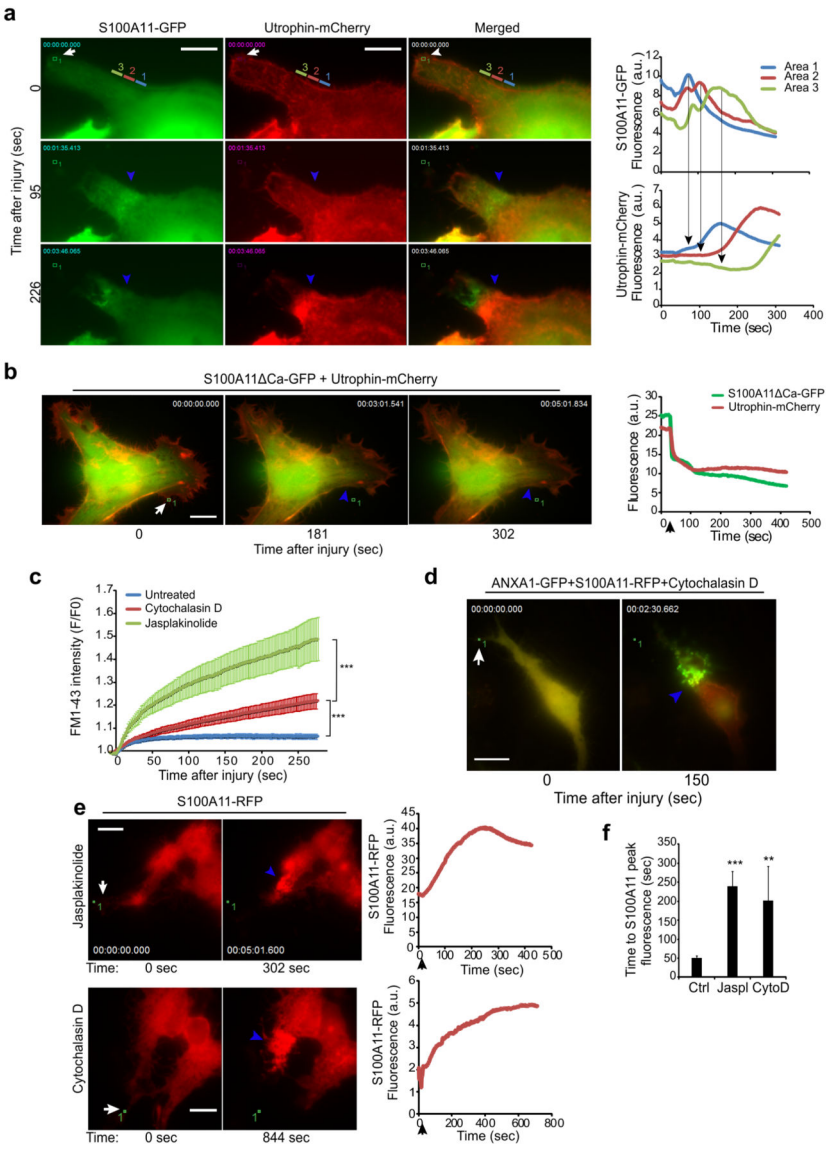

Figure 6. S100A11-ANXA2 complex augments PMR by altering local actin dynamics

(a) Images (*left)* of HeLa cells showing waves of recruitment of S100A11-GFP and F-actin (marked by Utrophin-mCherry) at the site of repair (areas 1-3) following laser injury (white arrow). Corresponding fluorescence intensity plots (*right*) reflect the presence of the indicated proteins in the colored areas marked 1, 2, and 3 before and after the injury. Supplementary Movie 7 shows the entire kinetics.

(b) Representative images (*left*) of S100A11ΔCa-GFP and Utrophin-mCherry recruitment to the repair site (blue arrowheads) in a HeLa cell following a local laser injury (white arrow). Corresponding plot (*right*) shows fluorescence intensity of the indicated proteins at the repair site.

(c) Kinetics of repair following focal laser injury of HeLa cells pretreated with 20 μM cytochalasin D for > 30 minutes or with 0.5 μM jasplakinolide for > 30 min, as measured by

FM1-43 dye uptake approach described in figure 2b. Each curve is an average of 10 cells. ***represent *P* Value < 10^{-3} (at 275 s) based on Students t-test.

(d) Image showing the extent of cell membrane injury as marked by ANXA1-GFP accumulation in a HeLa cell pretreated with cytochalasin D for 30 min prior to laser injury.

(e) Representative images (*left)* of HeLa cells expressing S100A11-RFP and treated with Jasplakinolide for 120 min or with Cytochalasin D for 80 min before laser injury. Corresponding plots show the kinetics of S100A11-RFP recruitment at the site of repair (blue arrowhead).

(f) Time for peak S100A11 accumulation at the repair site following laser injury of HeLa cells untreated (Ctrl) or treated as in (e). Error bars, SD for >5 independent experiments. The asterisks represent *P* Values based on Students t-test: ** *P* < 0,01; *** *P* < 0,001 when compared to untreated control cells. Scale bars, 20 μm.

Europe PMC Funders Author Manuscripts

Europe PMC Funders Author Manuscripts

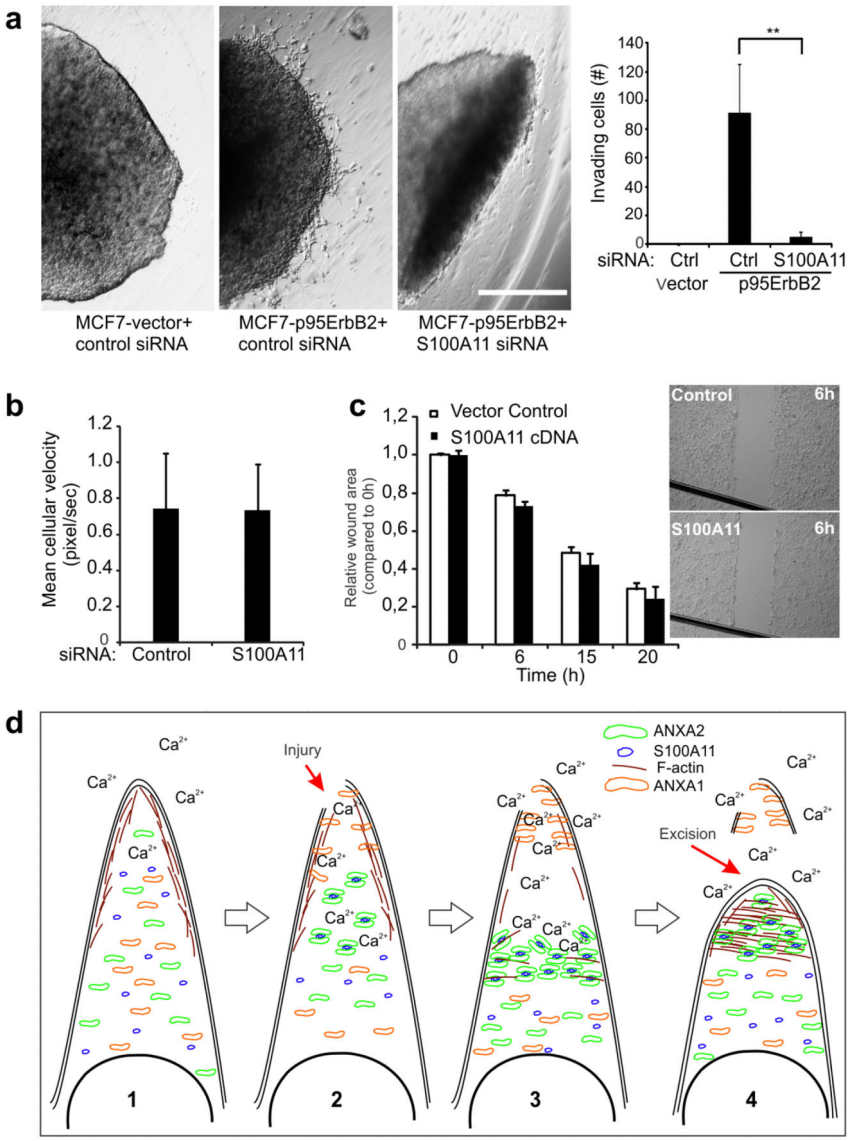

Figure 7. S100A11 is required for the invasiveness of MCF7-p95ErbB2 cells

(a) MCF7-vector and -p95ErbB2 cells expressing indicated siRNAs were grown in hanging drops overnight. Multicellular spheroids were subsequently grown for two days as spheroid cultures in a thin matrix of Matrigel. The spheroids were imaged with transmitted light to monitor the invasive growth of cells (*left*). Scale bar 1 mm. Plot (*right*) shows the quantification of invading cells from spheroids. Error bars represent SD for four independent spheroids. Based on Student's T-test ** represents *P* Value < 0.01.

(b) Sparsely seeded MCF7-p95ErbB2 cells treated with the indicated siRNAs for 72 hours were tracked for 6 hours. Mean cellular velocity was quantified for 30 cells in each condition; error bars represent SD. This data is representative of three independent experiments.

(c) Analysis of the directional motility of HeLa cells expressing S100A11 or empty vector (control). Confluent monolayer of HeLa cells was disrupted to generate a gap to facilitate

directional migration of cells. The edge of the gap in the monolayer (monolayer wound area) was quantified and wound distance calculated relative to 0 h. Inset shows representative images of monolayers after 6 h of cell migration. Error bars represent SD for three independent experiments. Scale bar, 1mm.

(d) Proposed model for cell membrane repair mediated by S100A11–ANXA2 complex. In uninjured cell: 1. Cortical actin maintains high tension of the plasma membrane and with the low cytosolic Ca^{2+} ANXA1, ANXA2 and S100A11 is distributed uniformly throughout the cytosol. 2. Local injury, 3. Causes increase in cytosolic Ca^{2+} resulting in accumulation of ANXA1 at the injury site, depolymerization of F-actin at this site and accumulation of S100A11-ANXA2 complex proximal to the injury site. 4. Actin depolymerization reduces the local membrane tension causing the wounded membrane surrounding the site of injury to collapse onto each other and separate from the damaged part of the cell membrane. The S100A11-ANXA2 complex initiates F-actin polymerization at this site which aids in the fusion of the injured membrane at the repair site and helps re-establish the membrane tension to support the newly formed cell membrane and facilitate complete wound closure.

Europe PMC Funders Author Manuscripts